

## Supporting Information

### **Elimination of Light-Induced Degradation at the Nickel Oxide-Perovskite Heterojunction by Aprotic Sulfonium Layer towards Long-Term Operationally Stable Inverted Perovskite Solar Cells**

Tianhao Wu,<sup>a</sup> Luis K. Ono,<sup>a</sup> Rengo Yoshioka,<sup>b</sup> Chenfeng Ding,<sup>a</sup> Congyang Zhang,<sup>a</sup> Silvia Mariotti,<sup>a</sup> Jiahao Zhang,<sup>a</sup> Kirill Mitrofanov,<sup>b</sup> Xiao Liu,<sup>c</sup> Hiroshi Segawa,<sup>c</sup> Ryota Kabe,<sup>b</sup> Liyuan Han,<sup>c, d</sup> Yabing Qi<sup>a, \*</sup>

<sup>a</sup> Energy Materials and Surface Sciences Unit (EMSSU), Okinawa Institute of Science and Technology Graduate University, 1919-1 Tancha, Onna-son, Kunigami-gun, Okinawa 904-0495, Japan

<sup>b</sup> Organic Optoelectronics Unit, Okinawa Institute of Science and Technology Graduate University, 1919-1 Tancha, Onna-son, Kunigami-gun, Okinawa 904-0495, Japan

<sup>c</sup> Special Division of Environmental and Energy Science, Komaba Organization for Educational Excellence (KOMEX), College of Arts and Sciences, University of Tokyo, Tokyo 153-8902, Japan

<sup>d</sup> State Key Laboratory of Metal Matrix Composites, School of Material Science and Engineering, Shanghai Jiao Tong University, Shanghai 200240, China

\*Corresponding author: Yabing Qi, E-mail: Yabing.Qi@OIST.jp

## Experimental procedures

### Materials

All chemicals were used without further purification, including PbI<sub>2</sub> (99.99%, TCI), PbBr<sub>2</sub> (99.99%, TCI), MAI (GreatCell Solar), MABr (GreatCell Solar), MACl (GreatCell Solar), FAI (GreatCell Solar), TMSBr (trimethylsulfonium bromide, Sigma-Aldrich), TMABr (tetramethylammonium bromide, Sigma-Aldrich), [6,6]-phenyl-C61-butyric acid methyl ester (PCBM, TCI), fullerene C<sub>60</sub> (TCI), bathocuproine (BCP, TCI), nickel acetylacetonate (95%, Sigma-Aldrich), poly(bis(4-phenyl)(2,4,6-trimethylphenyl)amine) (PTAA, TCI), magnesium acetate tetrahydrate (99%, TCI), Lithium carbonate (99%, TCI), acetonitrile (99.9%, Sigma-Aldrich), chlorobenzene (99.8%, Wako), ethanol (Wako), isopropanol (Wako), N,N-dimethylformamide (DMF, Wako), and dimethyl sulfoxide (DMSO, Wako).

### PSC fabrication

The FTO substrate was sequentially washed with distilled water, ethanol, acetone, and isopropanol. After being dried by N<sub>2</sub> flow, the substrate was treated by the ultraviolet light (UV)/O<sub>3</sub> for 35 min. After that, the substrate was transferred to the hotplate for deposition of NiO<sub>x</sub> layer. The precursor solution containing 20 mL nickel acetylacetonate with 15 mol% magnesium acetate tetrahydrate and 5 mol% lithium acetate in acetonitrile/ethanol (95:5/v:v) was sprayed onto the pre-heated FTO-coated glasses within 10 min at 550 °C by an air nozzle, and the substrates were kept at 550 °C for another 40 min to form compact NiO<sub>x</sub> film (about 15 nm in thickness). For the

deposition of PTAA layer on ITO substrate, 2 mg mL<sup>-1</sup> PTAA toluene solution was spin-coated onto the substrate at 6000 r.p.m. for 30 s, and then annealed at 120 °C for 20 min. Then, the substrates were transferred into a high-vacuum chamber (10<sup>-7</sup> Torr) after cooling down, the TMSBr layer with a controllable thickness was deposited on the NiO<sub>x</sub> substrate by thermal evaporation. Subsequently, a 1.35 M PbI<sub>2</sub> solution dissolved in DMF/DMSO (19:1, v/v) was spin-coated on the substrate at 3000 r.p.m. for 30 s in N<sub>2</sub> atmosphere. Next, a mixed organic cation solution (60 mg FAI, 20 mg MAI, and 5 mg MACl dissolved in 1 ml isopropanol) was spin-coated at 3000 r.p.m. for 30 s and then annealed at 150 °C for 10 min in air to form perovskite layer. For the fabrication of 1.66-eV bandgap perovskite, 1.1 M PbI<sub>2</sub> and 0.2 M PbBr<sub>2</sub> were dissolved in DMF/DMSO (19:1, v/v) solution and spin-coated at 3000 r.p.m. for 30 s, and a mixed organic cation solution (55 mg FAI, 15 mg MABr, and 8 mg MACl dissolved in 1 ml isopropanol) was spin-coated at 3000 r.p.m. for 30 s and then annealed at 150 °C for 10 min. Then, 0.1 mg mL<sup>-1</sup> organic D-π-A passivator (2-cyano-3-(5-(4-(dibutylamino)phenyl)thiophen-2-yl)acrylic acid) chloroform solution was spin-coated at 4000 r.p.m. for 20 s on the perovskite surface. Then, 5 mg mL<sup>-1</sup> PCBM chlorobenzene solution was spin-coated on the substrate at 1000 r.p.m. for 30 s and dried at 70 °C for 10 min. Finally, 20 nm C<sub>60</sub>, 5 nm BCP, and 80 nm silver electrode were evaporated onto the substrate under a high-vacuum condition (10<sup>-7</sup> Torr).

### **Sample characterization**

SEM measurements were carried out using a Helios NanoLab G3 scanning electron

microscope (FEI). X-ray diffraction measurements were carried out on a Bruker D8 Discover diffractometer (Bruker AXS) using a Cu ( $\lambda = 1.54 \text{ \AA}$ ) X-ray source with the power of 1600 W. The XPS spectra were recorded by a Kratos X-ray photoelectron spectrometer (AXIS Ultra HAS) equipped with monochromatic Al K $\alpha$  (1486.6 eV) source. The XPS plots were fitted by the Gaussian–Lorentzian functions after subtracting the background induced by inelastic scattering processes. The steady-state PL curves were obtained using a Hamamatsu C12132 fluorescence lifetime spectrometer (Japan) at an excitation wavelength of 400 nm. The SIMS (Kratos Axis ULTRA) equipped with a quadrupole mass spectrometer (HAL 7, Hiden Analytical) was used to collect the elemental signals in a positive ion detection mode in a high-vacuum chamber with a pressure of  $10^{-8}$  Torr, a 1 keV Ar<sup>+</sup> source was used for the sputtering process during SIMS measurement. Liquid-state <sup>1</sup>H NMR spectroscopy measurements was performed on a 500 MHz nuclear magnetic resonance spectrometer (Bruker) using d6-DMSO as deuterated solvent at the room temperature with an acquisition time of 4 s and 128 accumulations. Femtosecond transient absorption measurements were conducted using a home-made pump-probe system constructed using CMOS detector (S12198-1024Q, Hamamatsu) and InGaAs photodiode array (G9203-256DA, Hamamatsu). An Yb:KGW laser (Light conversion, Pharos, 1030 nm, 1 kHz repetition rate, 150 fs, 2 mJ per pulse) was used as the main light source. The output from the laser was split into the pump beam and probe beam. The pump beam was directed into the optical parametric amplifier (Light conversion, ORPHEUS) to generate the 343 nm excitation and the probe beam was focused into a YAG plate to

generate white light continuum. The absorbance of perovskite film was measured using a UV-Vis spectrometer (V-670, JASCO).

### **Time-resolved MS characterization**

The time-resolved MS measurement was conducted in our home-built vacuum chamber coupled with a solar simulator and temperature measurement system. The vacuum chamber with a background pressure of  $2 \times 10^{-8}$  Torr (CC-10, VISTA Corp.) is achieved by a turbo molecular pump (TMP; HiCube80, Pfeiffer). On the top part of the chamber, a quartz window is mounted where a simulated sun-light is illuminated using a 150 W Xe lamp from the solar simulator (PEC-L01, Peccell Technologies, Inc.). The illumination power delivered by the solar simulator was calibrated using a calibrated Si photodiode (Model 91150V, Oriel Instruments). The 5 cm  $\times$  5 cm substrates with perovskite films are fixed using a home-designed sample holder. A quadrupole mass spectrometer (HAL3F501RC, Hiden Analytical) with the  $m/z$  range of 1–510 amu and electron multiplier (to enhance signal detection) is mounted between the sample holder and TMP. The thermocouple wires are inserted into the vacuum chamber using electrical feedthrough and connected directly to the backside (glass side) of the samples allowing to acquire temperature profiles (RX-450K, AsOne Corp.) simultaneously with the mass spectrometry measurements. Regarding the release of toxic hydrogen cyanide during the tests, the MS system was connected to the gas exhaust system of the lab that handle toxic gases.

### **Trap density measurement**

The  $J$ - $V$  curves of the hole-only and electron-only devices were measured by a semiconductor characterization system (4200-SCS, Keithley) in dry N<sub>2</sub> with a voltage step of 10 mV. The trap density ( $N_{\text{trap}}$ ) can be deduced from  $V_{\text{TFL}}$  that is corresponding to the onset voltage of the trap-filled limit region, as shown in the following equation:

$$N_{\text{trap}} = \frac{2\varepsilon_0\varepsilon_r V_{\text{TFL}}}{qd^2} \quad (\text{Eqn. S1})$$

where  $\varepsilon_0$  is the vacuum permittivity,  $\varepsilon_r$  is the relative dielectric constant,  $q$  is the charge constant, and  $d$  is the thickness of the perovskite film (about 500 nm).

### **Photovoltaic characterization**

The  $J$ - $V$  plots of PSCs were measured under AM1.5G light illumination (100 mW cm<sup>-2</sup>, calibrated using a KG3 reference silicon cell (Enlitech)), using a solar simulator (Newport Oriel Sol 1A, xenon lamp, USHIO, UXL-150SO) and Keithley 2420 source meter in ambient air at around 25 °C and a relative humidity of 30% without preconditioning. A metal mask with an aperture area of 0.09 cm<sup>2</sup> was used during the device measurement. The IPCE spectra of the inverted PSCs were characterized using Oriel IQE 200 system.

### **Stability measurement**

For the continuous operational stability measurements, the devices were loaded in our home-designed enclosure box under dry N<sub>2</sub> flow to keep a relative humidity below 5% and a controllable temperature (from 65 °C to 25 °C by increasing the N<sub>2</sub> flow). The

PSCs were continuously illuminated by a solar simulator (Peccell PEC-L01) and Keithley 2401 source meter with the control of a LabView program to allow automatic measurements for a long time. To simulate operational condition of device, a fixed bias voltage close to the initial maximum power point voltage was applied to the PSCs during entire operational process. The power output was derived by the fixed bias and photocurrent recorded in the customized LabView program.

### **First-principles calculations**

Density functional theory (DFT) calculations were conducted on the Gaussian 09 program by using B3LYP with all-electron double- $\xi$  valence basis sets of 6-31G\*. Geometry optimizations of MA, FA, and TMS molecules were applied at the gas phase. Vibrational frequency calculations were employed to confirm that the optimized structures have no imaginary frequency. The lattice relaxation process of the TMSBr-terminated  $\text{FA}_{0.8}\text{MA}_{0.2}\text{PbI}_3$  (100) model connected on NiO (001) substrate was carried out in the framework of DFT method as implemented in the CASTEP program with a plane-wave kinetic energy cutoff of 400 eV.<sup>1-3</sup> Moreover, about 15 Å vacuum space was introduced on the top of the model surface to reduce the interaction between adjacent slabs. For calculation of total density of state of the models, we built the FAI-terminated and TMS-terminated  $\text{FAPbI}_3$  (100), (111), and (210) slabs with several layers of  $[\text{PbI}_6]^{4-}$  units and 20 Å vacuum space on the top to avoid the slab interaction. The generalized gradient approximation in the form of Perdew–Burke–Ernzerhof was used for the exchange–correlation function.



## Supplementary figures and tables

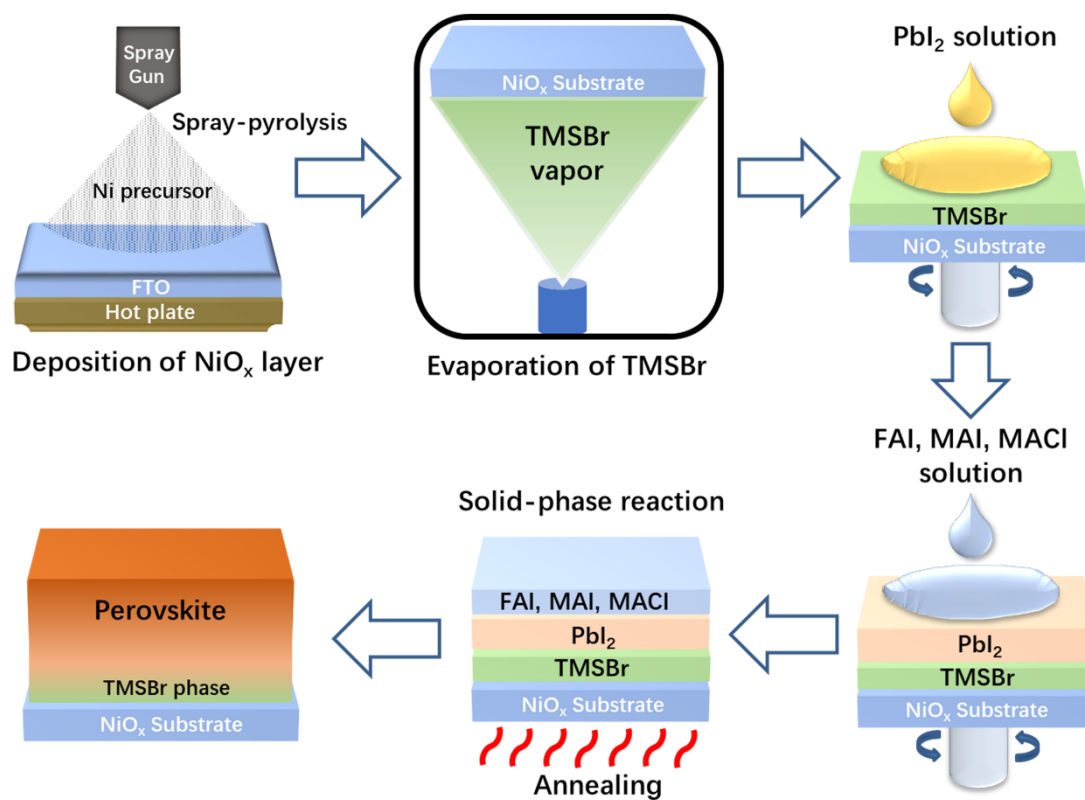


**Fig. S1** Illustration of the fabrication process of the NiO<sub>x</sub>-FAMAPbI<sub>3</sub> perovskite heterojunction with a TMSBr buffer layer.

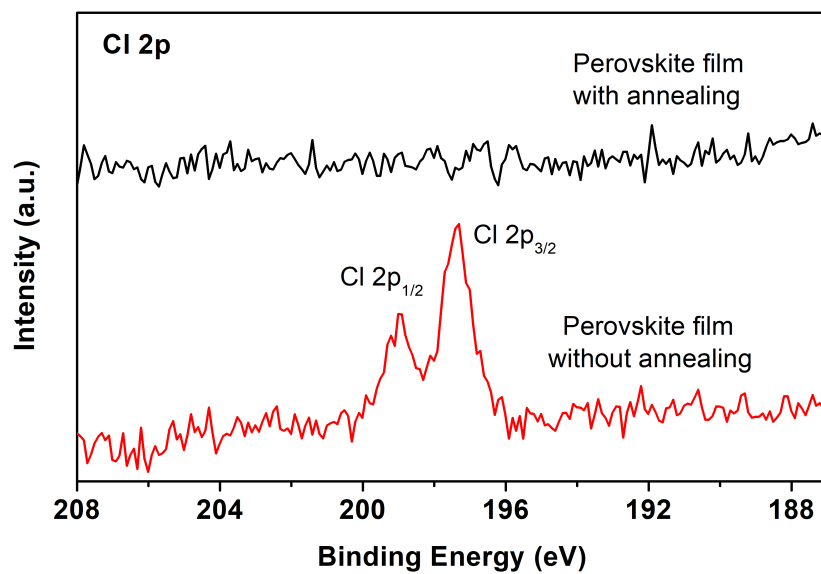


**Fig. S2** XPS spectra of the Cl 2p region of the perovskite films without or with annealing at 150 °C for 10 min.

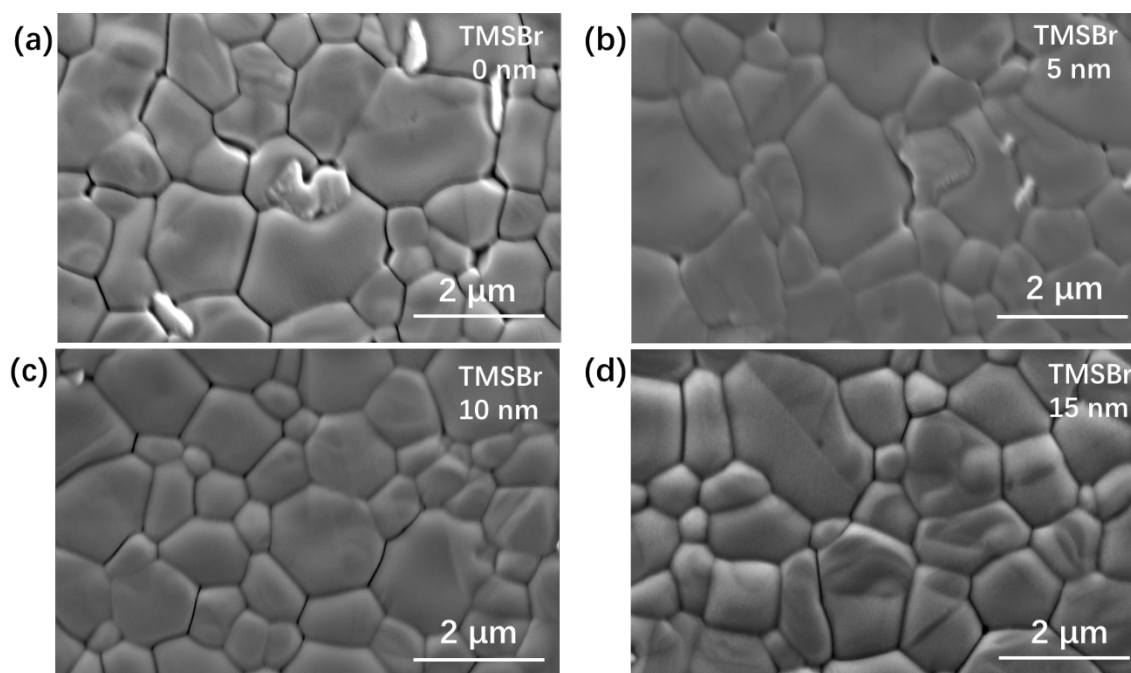


**Fig. S3** Top-view scanning electron microscopy (SEM) images of the perovskite films with an evaporated TMSBr film with a thickness of (a) 0 nm, (b) 5 nm, (c) 10 nm, and (d) 15 nm during film fabrication.

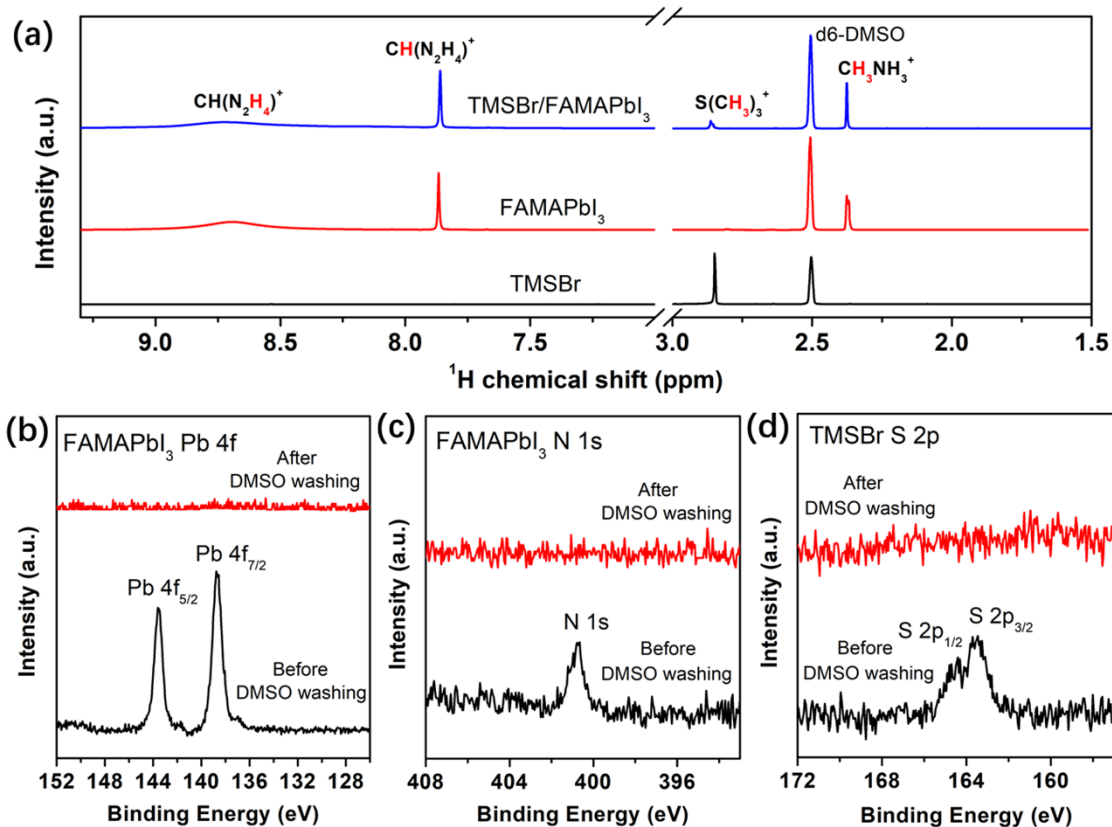


**Fig. S4** (a) Liquid-state proton nuclear magnetic resonance ( $^1\text{H}$  NMR) spectra of the TMSBr, FAMAPbI<sub>3</sub>, and TMSBr/FAMAPbI<sub>3</sub> samples. The characteristic peak of the d6-DMSO solvent was detected at 2.5 ppm. XPS high-resolution spectra of the (b) Pb 4f and (c) N 1s regions of the FAMAPbI<sub>3</sub> perovskite film on NiO<sub>x</sub> substrate before and after the DMSO washing process. (d) XPS high-resolution spectra of the S 2p region of the TMSBr film on NiO<sub>x</sub> substrate before and after the DMSO washing process.

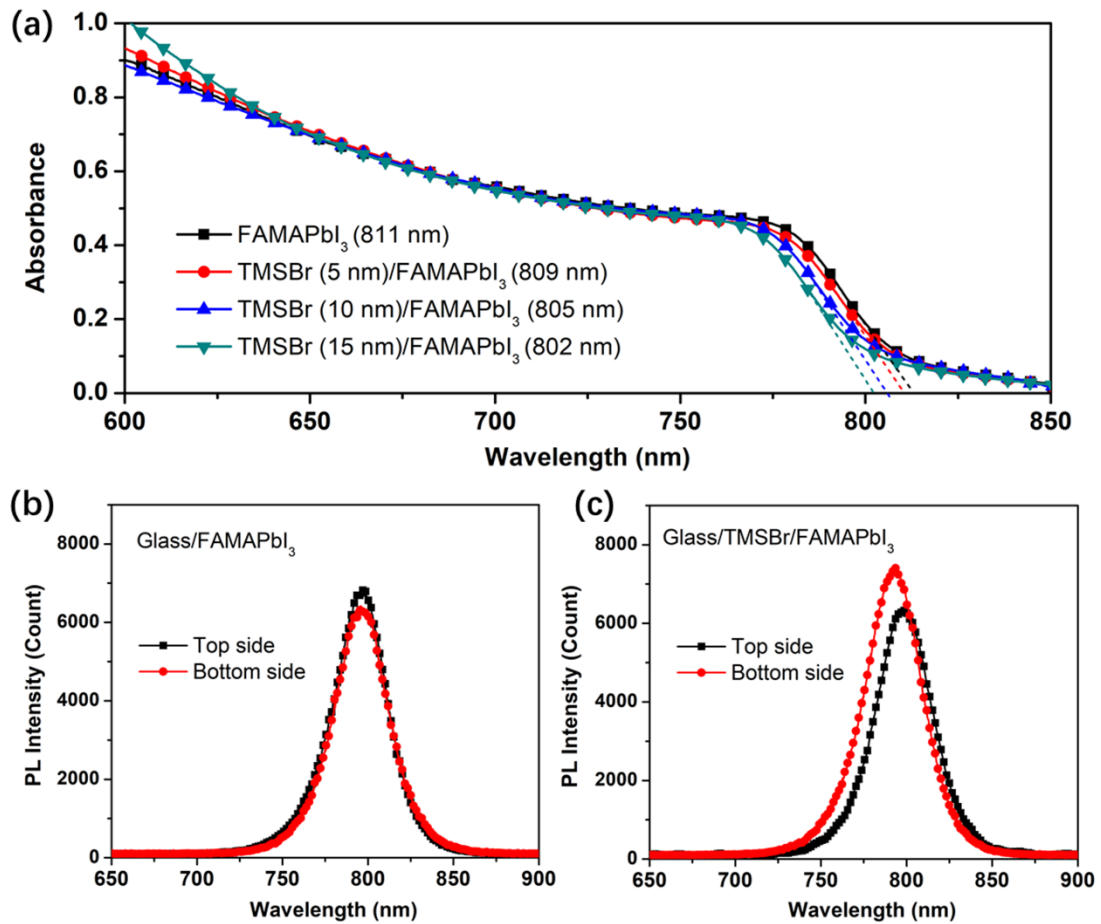


**Fig. S5** (a) UV-vis absorption spectra of the FAMAPbI<sub>3</sub> films incorporated with different thickness of TMSBr. (b and c) The steady-state photoluminescence (PL) spectra of the FAMAPbI<sub>3</sub> and TMSBr(10 nm)/FAMAPbI<sub>3</sub> film deposited on glass substrate with the incident from perovskite side (top side) and glass side (bottom side).

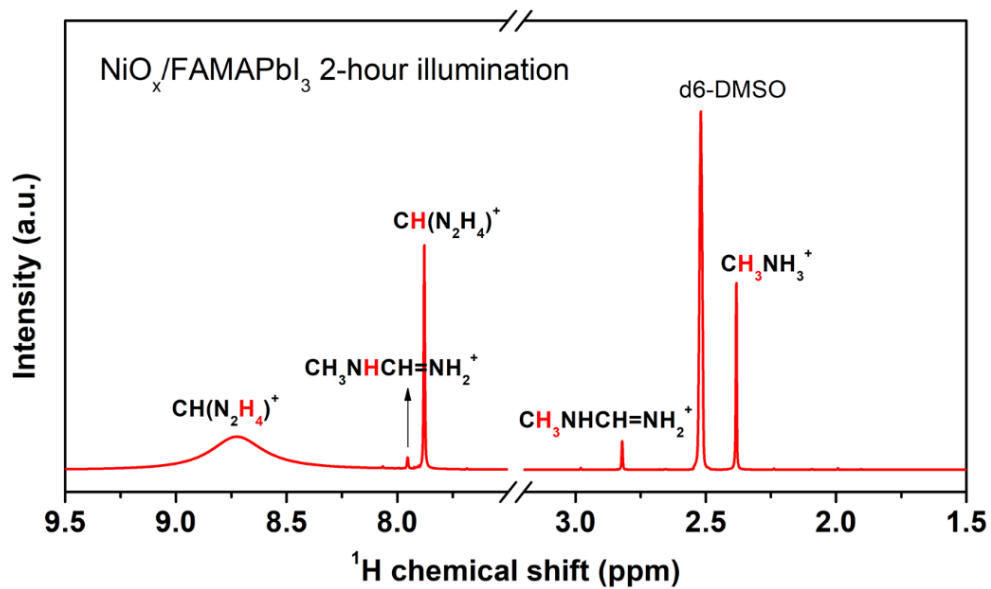


**Fig. S6** Liquid-state  $^1\text{H}$  NMR spectrum of the  $\text{NiO}_x/\text{FAMAPbI}_3$  sample measured after 1-sun illumination for 2 hours.

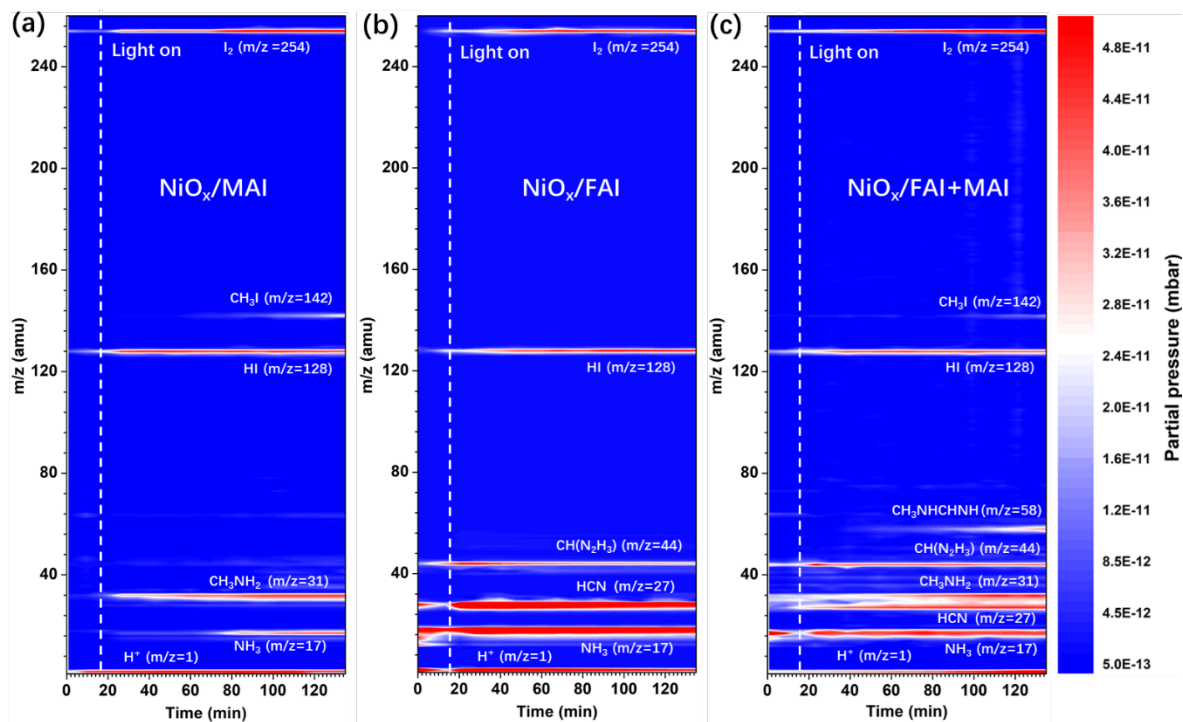


**Fig. S7** Time-resolved MS contour plots ( $m/z = 1\text{--}260$  amu) of (a)  $\text{NiO}_x/\text{MAI}$ , (b)  $\text{NiO}_x/\text{FAI}$ , and (c)  $\text{NiO}_x/(\text{FAI}+\text{MAI})$  films (FAI/MAI ratio = 0.8/0.2) coated on glass substrate. The simulated 1-sun light was applied after 15 min of the MS measurement.

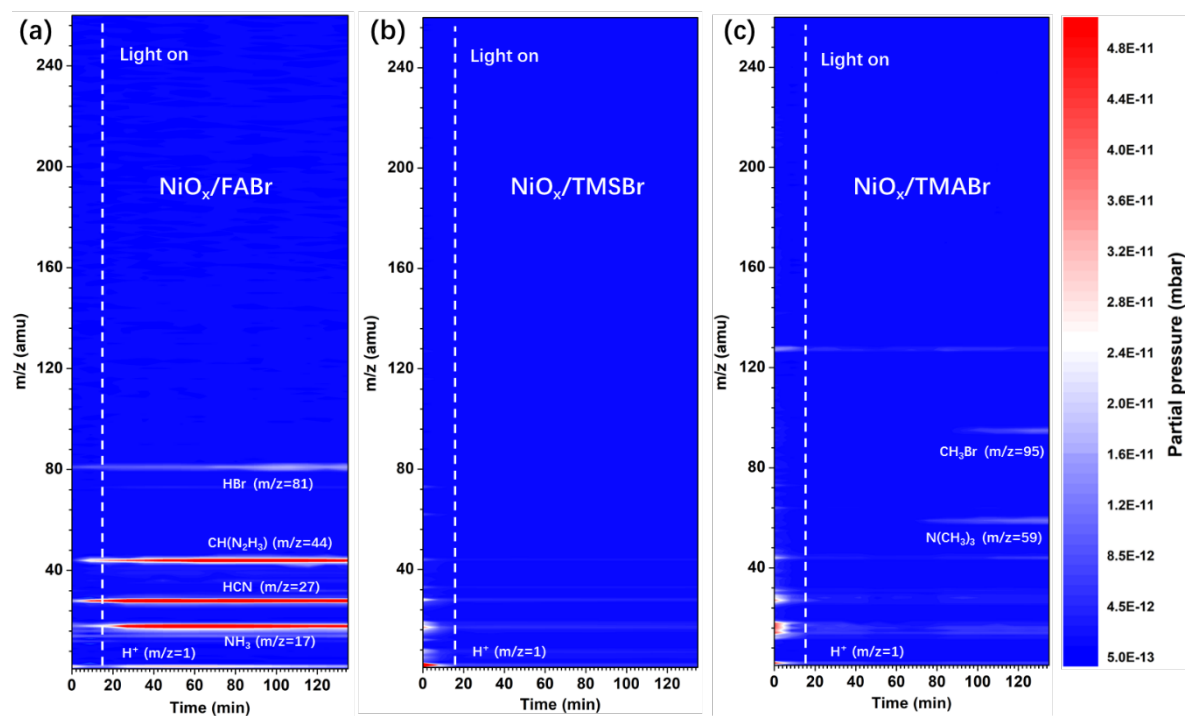


**Fig. S8** Time-resolved MS contour plots ( $m/z = 1\text{--}260$  amu) of (a)  $\text{NiO}_x/\text{FABr}$ , (b)  $\text{NiO}_x/\text{TMSBr}$ , and (c)  $\text{NiO}_x/\text{TMABr}$  films (fabricated by vapor deposition) coated on FTO glass substrates. The simulated 1-sun light was applied after 15 min of the MS measurement.

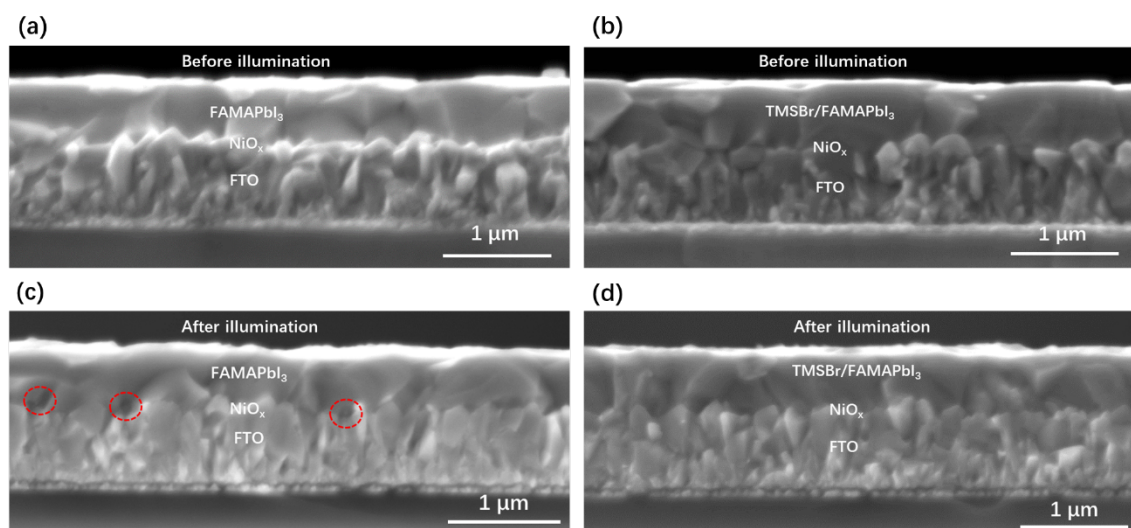


**Fig. S9** (a and b) Cross-section SEM images of the NiO<sub>x</sub>/FAMAPbI<sub>3</sub> and NiO<sub>x</sub>/TMSBr/FAMAPbI<sub>3</sub> films before illumination. (c and d) Cross-section SEM images of the NiO<sub>x</sub>/FAMAPbI<sub>3</sub> and NiO<sub>x</sub>/TMSBr/FAMAPbI<sub>3</sub> films after illumination for 2 hours in MS measurement, and the red circles indicate the pinholes formed at the NiO<sub>x</sub>/perovskite interface.

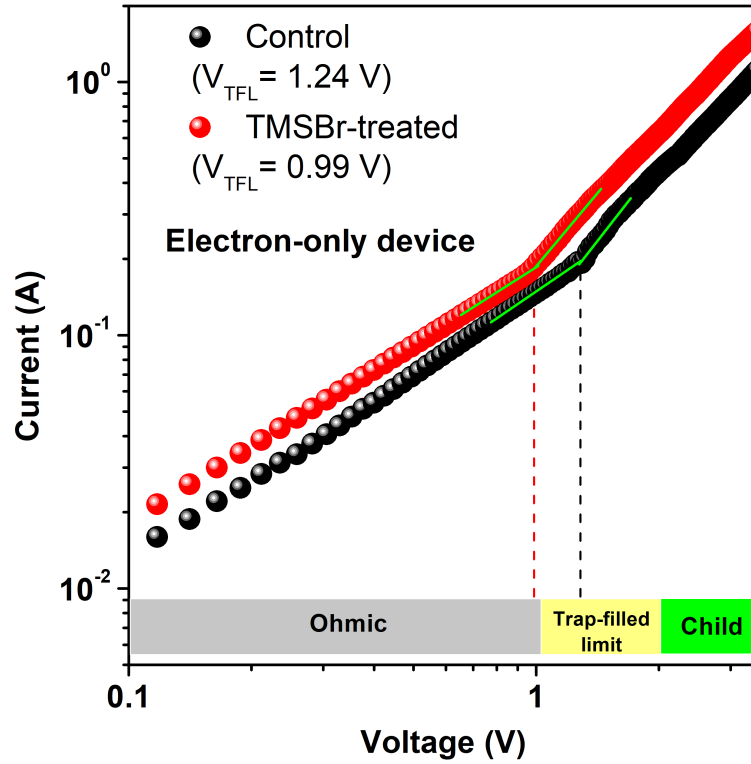


**Fig. S10** Dark current plots of the electron-only devices (FTO/C<sub>60</sub>/perovskite/C<sub>60</sub>/Ag) with or without TMSBr treatment, three regions can be identified according to different values of the slope  $n$ :  $n = 1$  is the Ohmic region,  $n = 2$  is the SCLC region (Child), and  $n > 2$  is the trap-filled limited region.

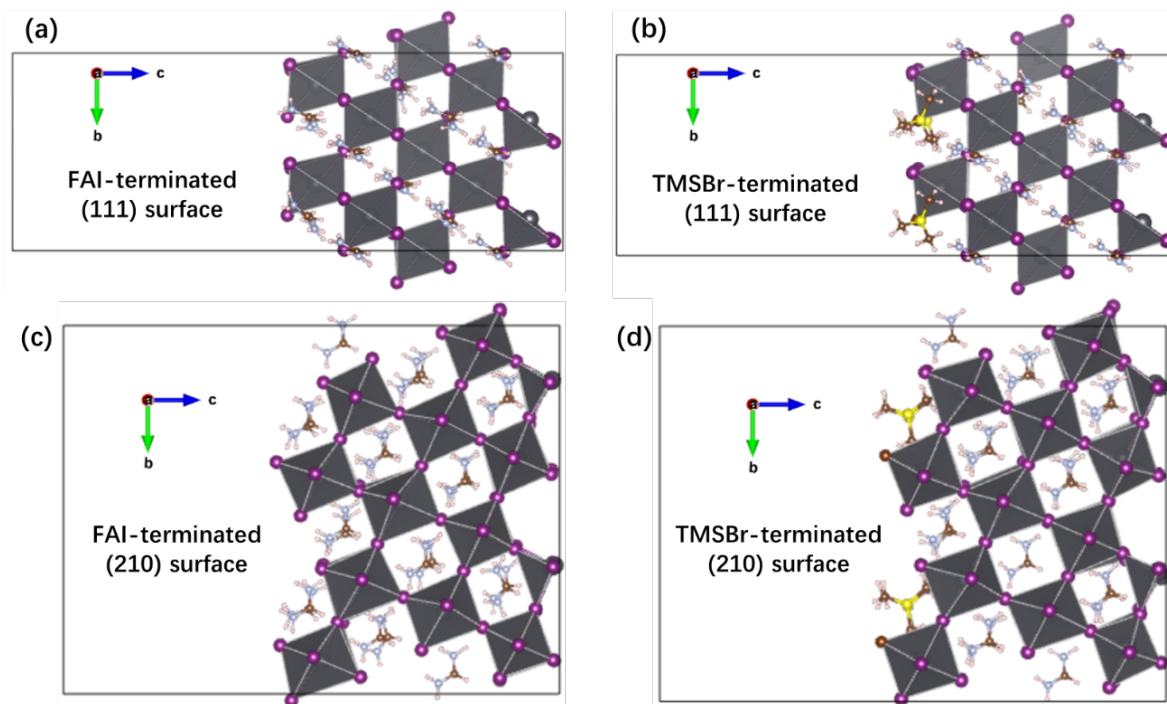


**Fig. S11** (a and c) FAI-terminated FAPbI<sub>3</sub> (111) and (210) slabs after relaxation to the minimum energy. (b and d) TMSBr-terminated FAPbI<sub>3</sub> (111) and (210) slabs after relaxation to the minimum energy. The white, brown, blue, yellow, gray, and purple spheres represent H, C, N, S, Pb, and I atoms, respectively.

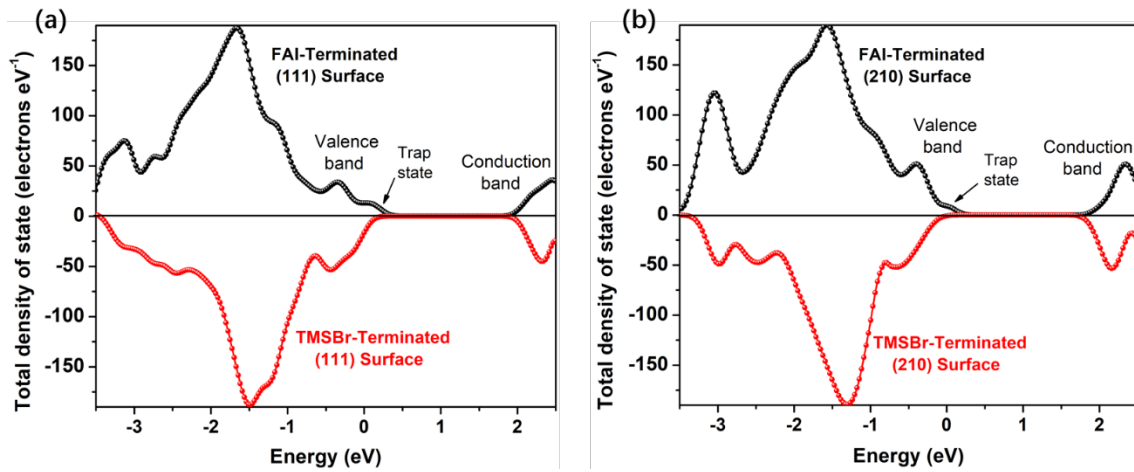


**Fig. S12** Total density of state distribution plots of the FAI-terminated and TMSBr-terminated FAPbI<sub>3</sub> (a) (111) slabs and (b) (210) slabs. The increased density of state at the valence band edge indicates the formation of hole trap states at the FAI-terminated surface.

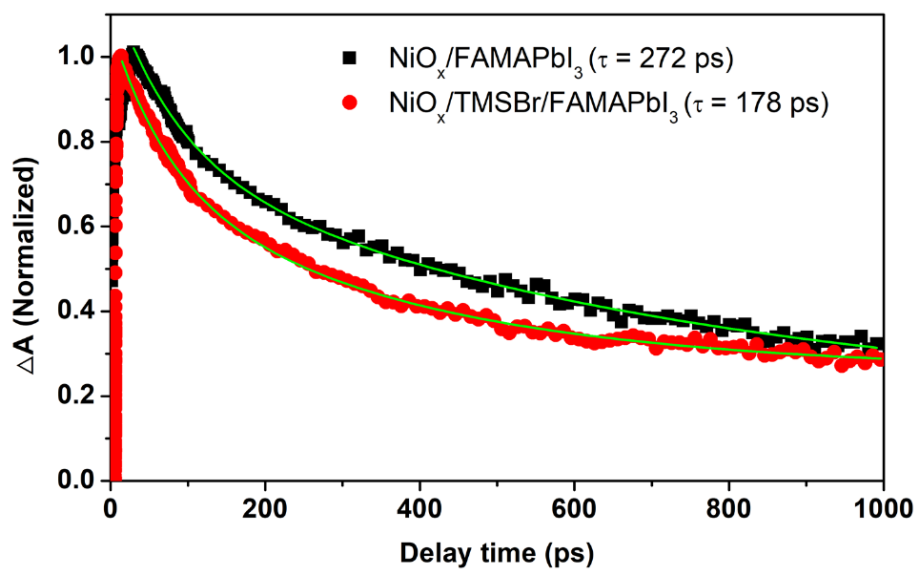


**Fig. S13** Transient absorption dynamics of the ground-state bleaching peaks of  $\text{NiO}_x/\text{FAMAPbI}_3$  and  $\text{NiO}_x/\text{TMSBr}/\text{FAMAPbI}_3$  films at a time scale of 0.1–1000 ps, and the decay lifetimes were calculated to be 272 ps and 178 ps, respectively.

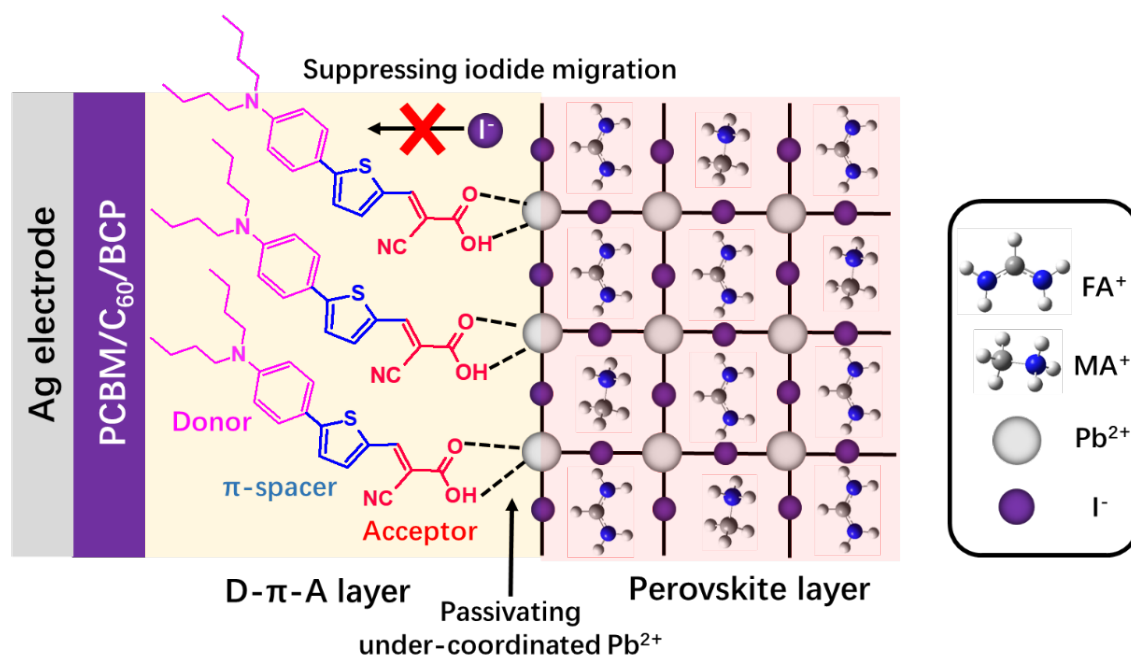


**Fig. S14** Schematic illustration of the passivation mechanism of under-coordinated  $\text{Pb}^{2+}$  defects on  $\text{FAMAPbI}_3$  perovskite surface by the donor- $\pi$ -acceptor type molecule, 2-cyano-3-(5-(4-(dibutylamino)phenyl)thiophen-2-yl)acrylic acid, which was synthesized according to our previous report.<sup>4</sup>

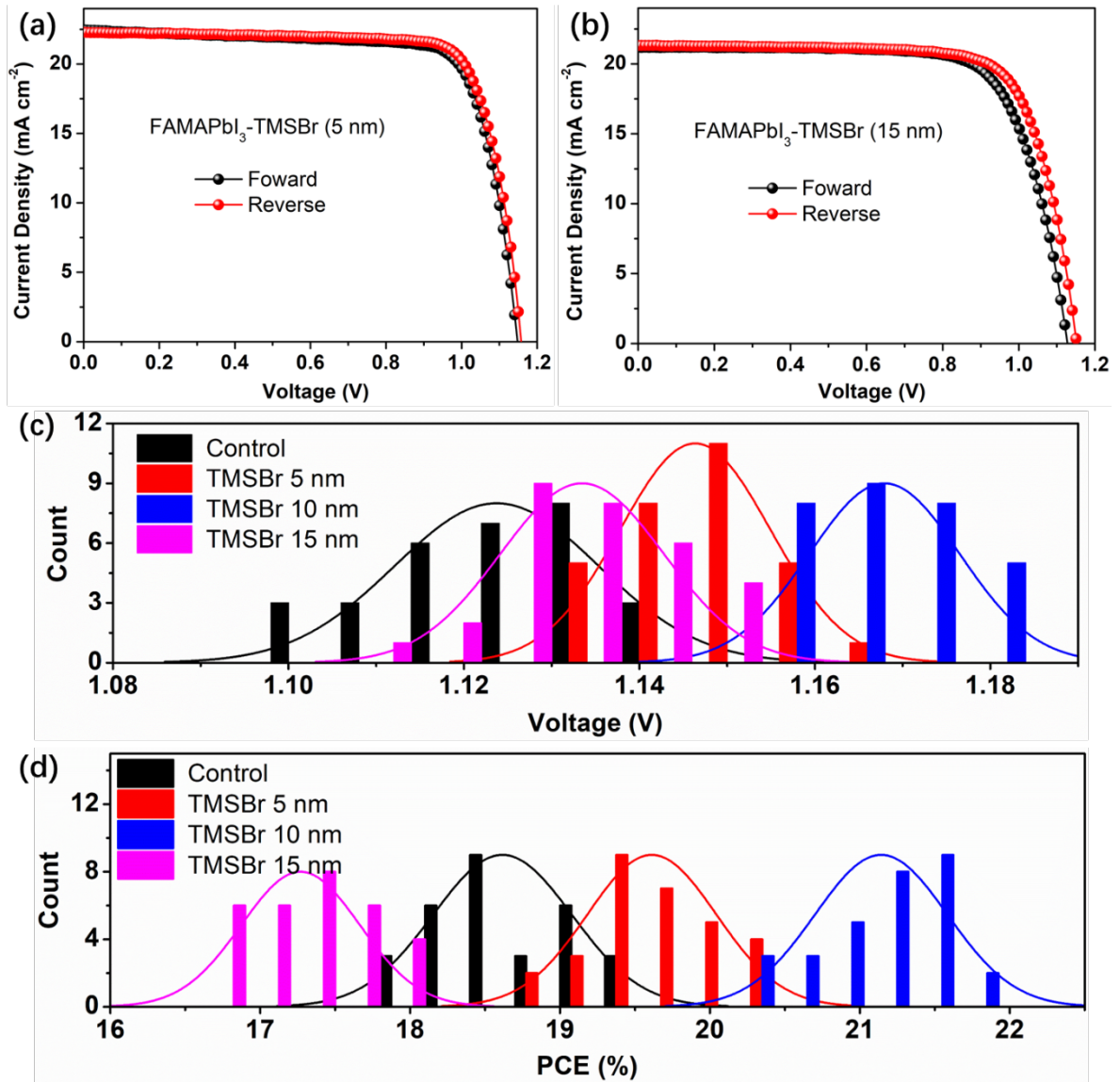


**Fig. S15**  $J-V$  curves of the inverted PSCs based on FAMAPbI<sub>3</sub> absorber with (a) 5 nm and (b) 15 nm TMSBr treatment. Statistical distribution of the (c)  $V_{OC}$  and (d) PCE for the corresponding PSC samples based on 30 individual cells.

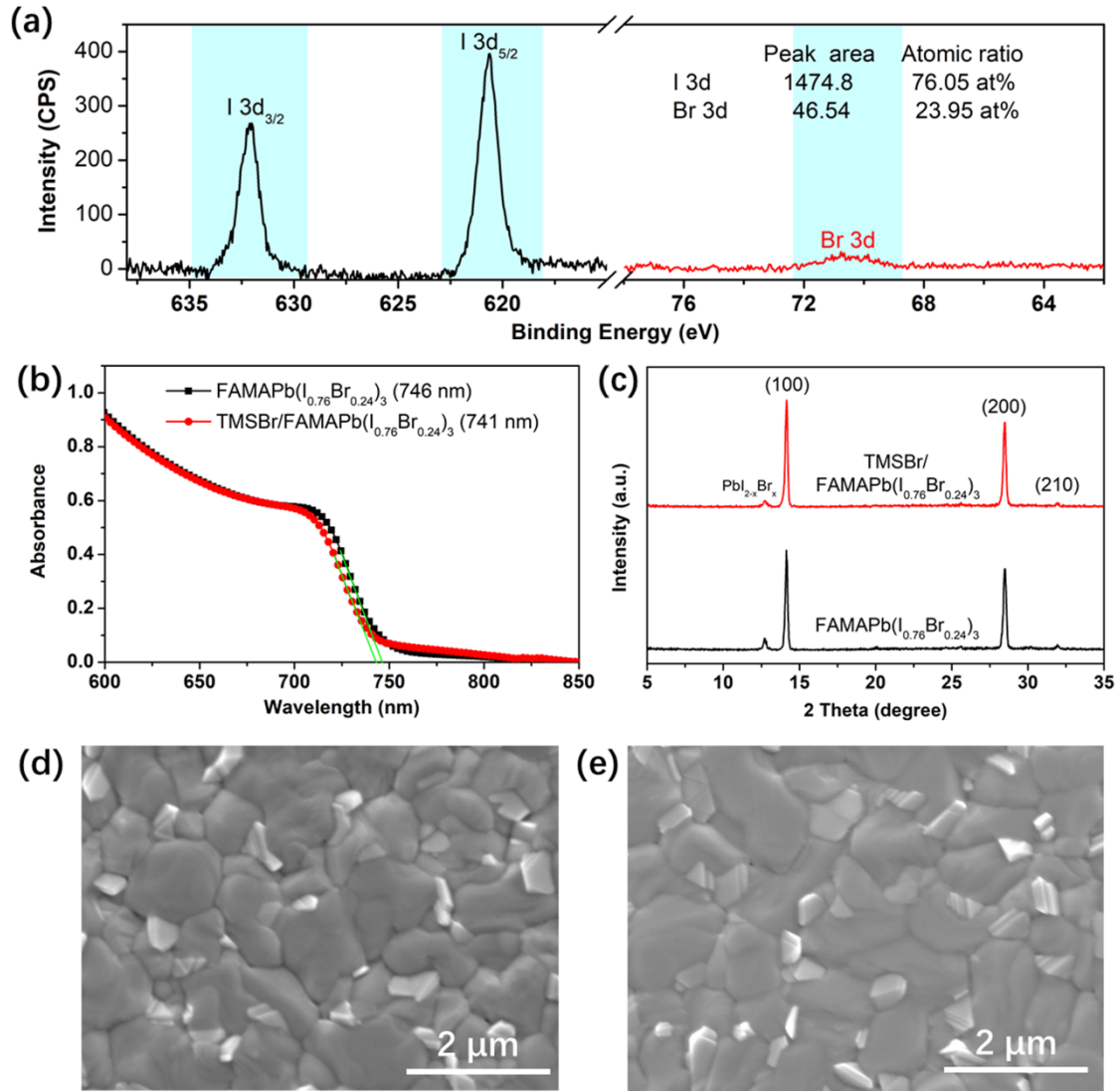


**Fig. S16** (a) XPS I 3d and Br 3d spectra of the wide-bandgap perovskite with the calculated I/Br ratio of 0.76/0.24. (b) UV-vis absorption spectra of the FAMAPb(I<sub>0.76</sub>Br<sub>0.24</sub>)<sub>3</sub> films without and with TMSBr (10 nm). (c) XRD patterns of the of the FAMAPb(I<sub>0.76</sub>Br<sub>0.24</sub>)<sub>3</sub> films without and with TMSBr. Top-view SEM images of the FAMAPb(I<sub>0.76</sub>Br<sub>0.24</sub>)<sub>3</sub> films (d) without and (e) with TMSBr.

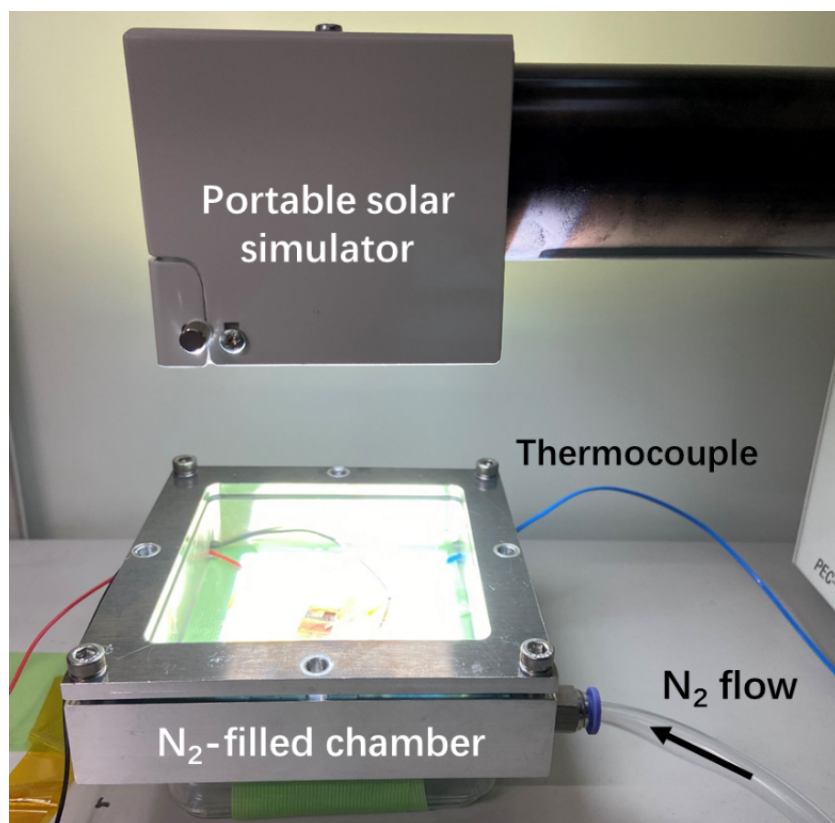


**Fig. S17** Test system for the operational stability measurement of PSCs. The temperature of testing device is monitored by a thermocouple (blue line), and additional N<sub>2</sub> flow was put into the sample chamber to keep the PSC temperature at a fixed value for both 65 °C and room temperature (RT) measurements.

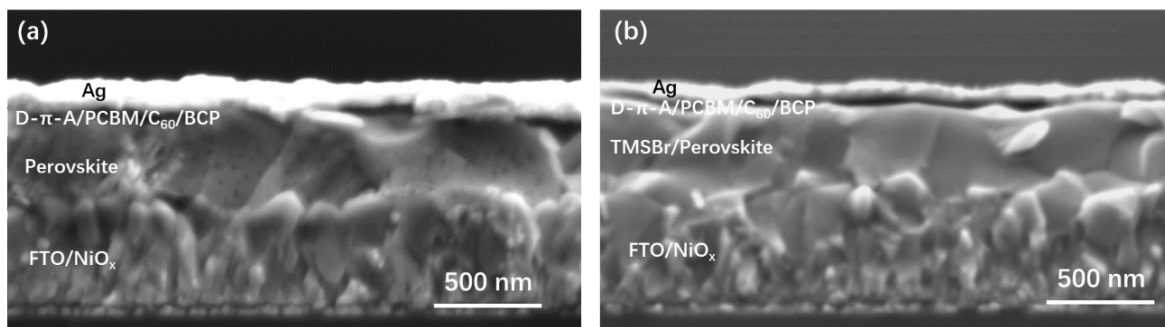


**Fig. S18** Cross-section SEM images of (a) the NiO<sub>x</sub>/perovskite and (b) NiO<sub>x</sub>/TMSBr/perovskite

PSCs after the operational stability test at 65 °C.

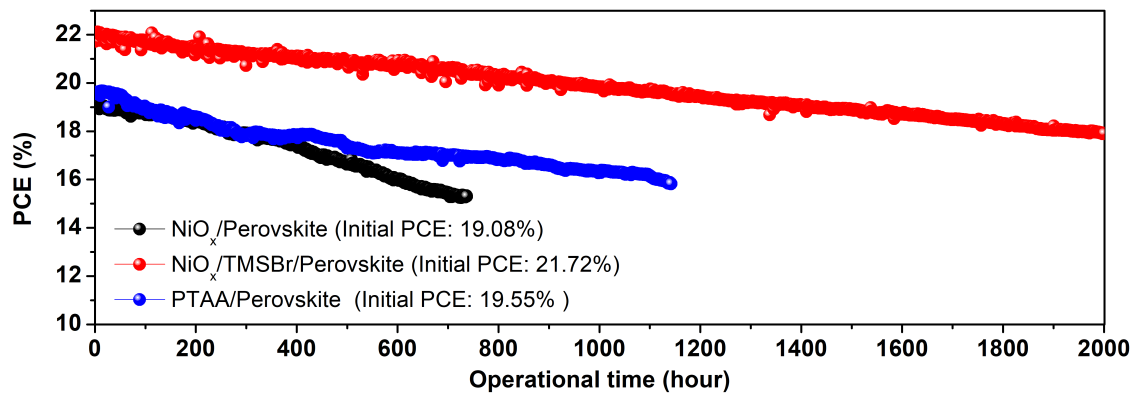


**Fig. S19** Actual PCE decay plots of the corresponding PSCs (representing the performance of champion device) measured under 1-sun illumination at 25 °C with a fixed bias near the maximum power point.

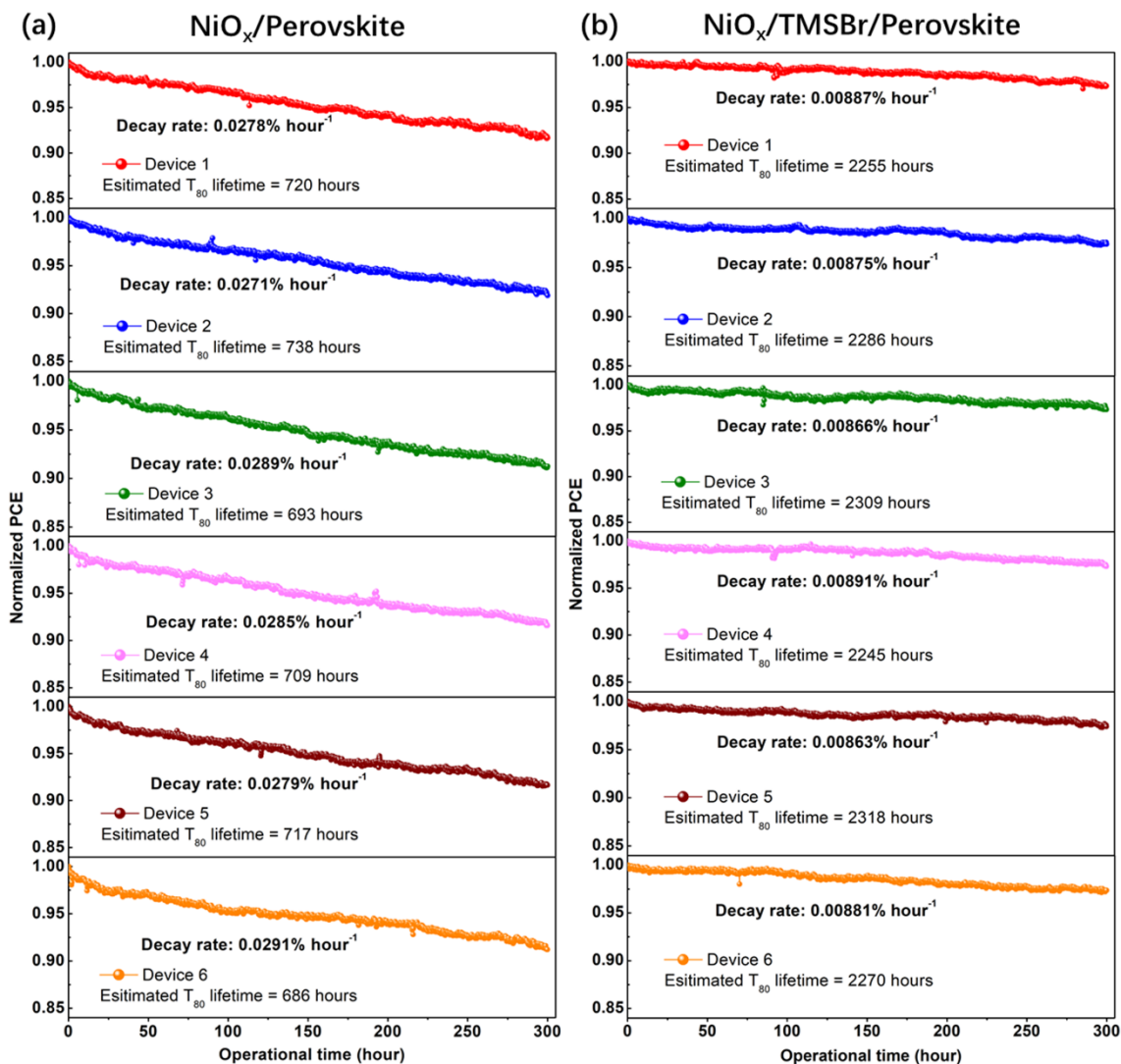


**Fig. S20** Stability reproducibility test of the (a) NiO<sub>x</sub>/Perovskite and (b) NiO<sub>x</sub>/TMSBr/Perovskite PSCs based on the results of 6 individual cells, all the devices operated under the same condition (1-sun illumination at 25 °C with dry N<sub>2</sub> flow). The T<sub>80</sub> lifetimes were calculated to be (7.1 ± 0.3)×100 hours for NiO<sub>x</sub>/Perovskite and (22.8 ± 0.4)×100 hours for the NiO<sub>x</sub>/TMSBr/Perovskite PSCs.

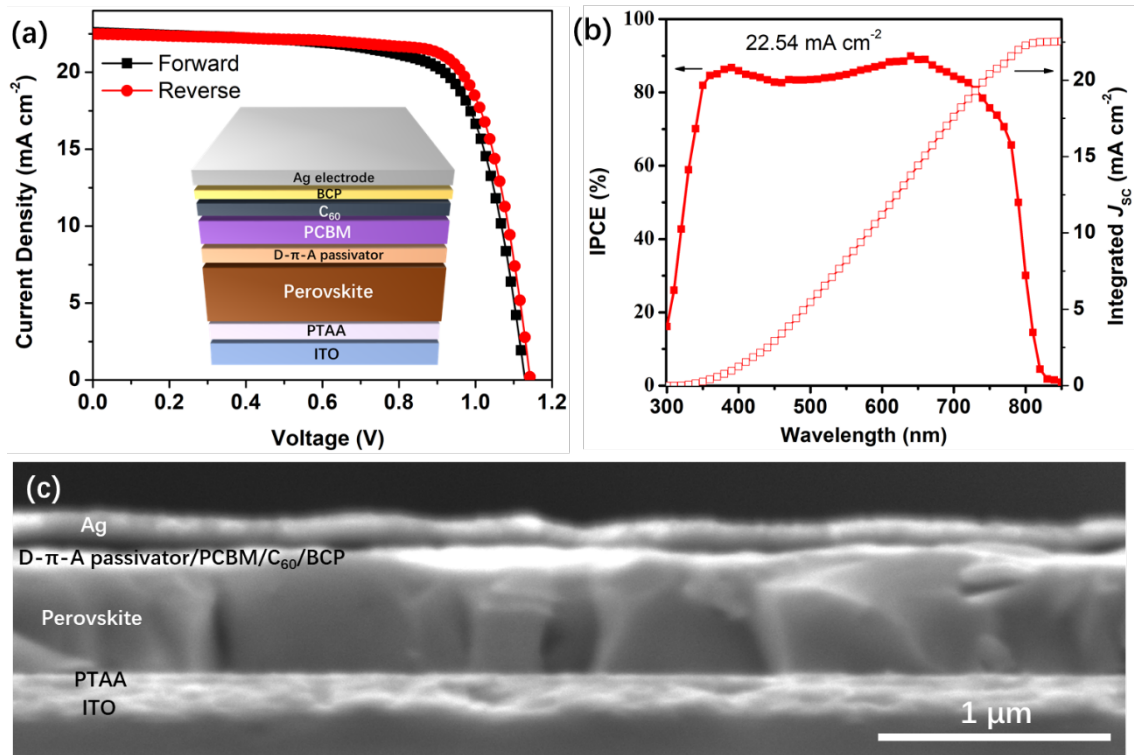


**Fig. S21** (a)  $J$ - $V$  curves of the inverted PSCs with a structure of ITO/PTAA/FAMAPbI<sub>3</sub> perovskite/D- $\pi$ -A passivator/PCBM/ $\text{C}_{60}$ /BCP/Ag. (b) IPCE spectrum of the PTAA-based device. (c) Cross-section SEM image of the PTAA-based inverted PSCs.

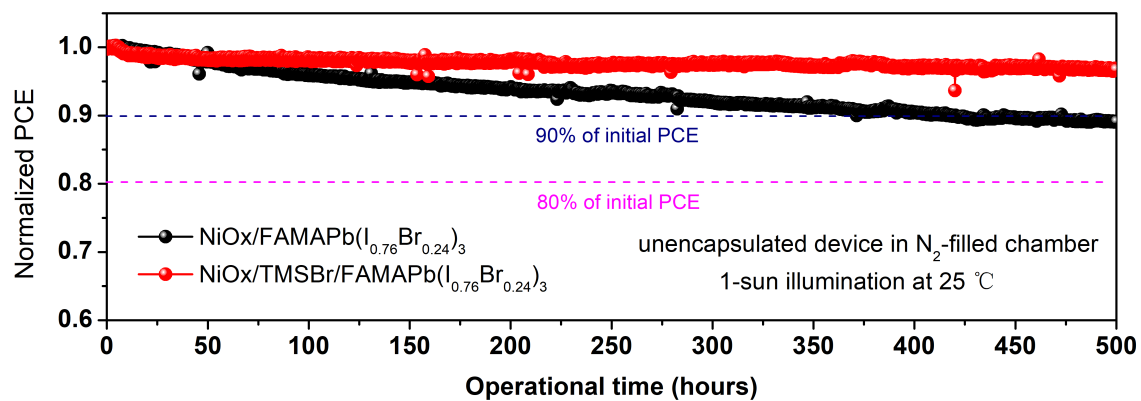


**Fig. S22** PCE decay plots of the wide-bandgap inverted PSCs (representing the performance of champion device) measured under 25 °C and simulated 1-sun illumination at a fixed bias near the maximum power point.

**Table S1.** Photovoltaic parameters of the FAMAPbI<sub>3</sub> inverted PSCs with 5 nm and 10 nm TMSBr buffer layer on the NiO<sub>x</sub>/perovskite interface.

Perovskite	Scan	$J_{sc}$	$V_{oc}$	FF	PCE
	Direction	[mA cm <sup>-2</sup> ]	[V]	[%]	[%]
FAMAPbI <sub>3</sub> -TMSBr (5 nm)	forward	22.43	1.15	76.71	19.79
	reverse	22.29	1.16	78.56	20.31
FAMAPbI <sub>3</sub> -TMSBr (15 nm)	forward	21.19	1.12	71.92	17.07
	reverse	21.31	1.15	73.56	18.03

Table S2 Summary of the efficiency and the operational lifetime (under 1-sun illumination and maximum power point) reported from the state-of-the-art NiO<sub>x</sub>-based inverted PSCs, the test conditions including temperature and relative humidity (RH) values are also presented.

Perovskite Composition	Hole Transport Materials	Efficiency [%]	Operational Lifetime	Test Condition	Ref.
Cs <sub>0.05</sub> (MA <sub>0.15</sub> FA <sub>0.85</sub> ) 0.95Pb(I <sub>0.85</sub> Br <sub>0.15</sub> ) <sub>3</sub>	NiO <sub>x</sub>	22.6	T <sub>92</sub> = 1000 hours (45 °C)	Encapsulated device in ambient air	5
Cs <sub>0.15</sub> FA <sub>0.85</sub> Pb (I <sub>0.95</sub> Br <sub>0.05</sub> ) <sub>3</sub>	NiO <sub>x</sub>	20.9	T <sub>95</sub> = 500 hours (65 °C) (white LED light source)	Encapsulated device in ambient air	6
Cs <sub>0.05</sub> MA <sub>0.1</sub> FA <sub>0.85</sub> PbI <sub>3</sub>	NiO <sub>x</sub>	23.1	T <sub>92</sub> = 500 hours (65 °C) (white LED light source)	Encapsulated device at 50% RH	7
CsFAMAPbI <sub>3</sub>	NiO <sub>x</sub> /PTAA	21.9	T <sub>85</sub> = 1000 hours (Room Temperature)	Unencapsulated device in N <sub>2</sub> atmosphere	8
Cs <sub>0.05</sub> MA <sub>0.16</sub> FA <sub>0.79</sub> Pb (Br <sub>0.16</sub> I <sub>0.86</sub> ) <sub>3</sub>	NiO <sub>x</sub>	19.7	T <sub>80</sub> = 500 hours (55 °C)	Unencapsulated device in N <sub>2</sub> atmosphere	9
(FAPbI <sub>3</sub> ) <sub>0.85</sub> (MAPbBr <sub>3</sub> ) <sub>0.15</sub>	NiO <sub>x</sub>	20.7	T <sub>80</sub> = 160 hours (Room Temperature)	Encapsulated device at 35% RH	10
MAPbI <sub>3</sub>	NiO <sub>x</sub>	20.2	T <sub>85</sub> = 720 hours (Room Temperature)	Unencapsulated device in N <sub>2</sub> atmosphere	11
MA <sub>0.89</sub> DMA <sub>0.11</sub> PbI <sub>3</sub>	NiO <sub>x</sub>	21.3	T <sub>80</sub> = 800 hours (Room Temperature, white LED light source)	Encapsulated device at 25% RH	12
CsFAMAPbI <sub>3</sub>	NiO <sub>x</sub>	22.1	T <sub>98</sub> = 1000 hours (45 °C) (white LED light source)	Encapsulated device at 25% RH	13
TMSBr/FAMAPbI <sub>3</sub>	NiO <sub>x</sub>	22.1	T <sub>88</sub> = 1000 hours (65 °C) T <sub>80</sub> = 2310 hours (Room Temperature)	Unencapsulated device in dry N <sub>2</sub> atmosphere	This work

**Table S3.** Photovoltaic parameters of the FAMAPbI<sub>3</sub> inverted PSCs based on a PTAA hole transport layer (HTL). Other functional layers are the same as the NiO<sub>x</sub>-based device.

Perovskite	Scan	$J_{sc}$	$V_{oc}$	FF	PCE
	Direction	[mA cm <sup>-2</sup> ]	[V]	[%]	[%]
FAMAPbI <sub>3</sub> (PTAA HTL-based device)	forward	22.65	1.13	74.26	19.01
	reverse	22.61	1.14	75.83	19.55

## References

1. P. E. Blöchl, *Phys. Rev. B*, 1994, **50**, 17953-17979.
2. G. Kresse and J. Furthmüller, *Comput. Mater. Sci.*, 1996, **6**, 15-50.
3. G. Kresse and J. Furthmüller, *Phys. Rev. B*, 1996, **54**, 11169-11186.
4. S. Zhang, A. Islam, X. Yang, C. Qin, K. Zhang, Y. Numata, H. Chen and L. Han, *J. Mater. Chem. A*, 2013, **1**, 4812-4819.
5. S. Wang, Y. Li, J. Yang, T. Wang, B. Yang, Q. Cao, X. Pu, L. Etgar, J. Han, J. Zhao, X. Li and A. Hagfeldt, *Angew. Chem. Int. Edit.*, 2022, **61**, 202116534.
6. S. Liu, R. Chen, X. Tian, Z. Yang, J. Zhou, F. Ren, S. Zhang, Y. Zhang, M. Guo, Y. Shen, Z. Liu and W. Chen, *Nano Energy*, 2022, **94**, 106935.
7. H. Chen, S. Teale, B. Chen, Y. Hou, L. Grater, T. Zhu, K. Bertens, S. M. Park, H. R. Atapattu, Y. Gao, M. Wei, A. K. Johnston, Q. Zhou, K. Xu, D. Yu, C. Han, T. Cui, E. H. Jung, C. Zhou, W. Zhou, A. H. Proppe, S. Hoogland, F. Laquai, T. Filleter, K. R. Graham, Z. Ning and E. H. Sargent, *Nat. Photonics*, 2022, **16**, 352-358
8. Y. Wang, H. Ju, T. Mahmoudi, C. Liu, C. Zhang, S. Wu, Y. Yang, Z. Wang, J. Hu, Y. Cao, F. Guo, Y.-B. Hahn and Y. Mai, *Nano Energy*, 2021, **88**, 106285.
9. C. C. Boyd, R. C. Shallcross, T. Moot, R. Kerner, L. Bertoluzzi, A. Onno, S. Kavadiya, C. Chosy, E. J. Wolf, J. Werner, J. A. Raiford, C. de Paula, A. F. Palmstrom, Z. J. Yu, J. J. Berry, S. F. Bent, Z. C. Holman, J. M. Luther, E. L. Ratcliff, N. R. Armstrong and M. D. McGehee, *Joule*, 2020, **4**, 1759-1775.
10. W. Chen, Y. Wang, G. Pang, C. W. Koh, A. B. Djurišić, Y. Wu, B. Tu, F.-z. Liu, R. Chen, H. Y. Woo, X. Guo and Z. He, *Adv. Funct. Mater.*, 2019, **29**, 1808855.
11. J. Zhang, J. Long, Z. Huang, J. Yang, X. Li, R. Dai, W. Sheng, L. Tan and Y. Chen, *Chem. Eng. J.*, 2021, **426**, 131357.
12. H. Chen, Q. Wei, M. I. Saidaminov, F. Wang, A. Johnston, Y. Hou, Z. Peng, K. Xu, W. Zhou, Z. Liu, L. Qiao, X. Wang, S. Xu, J. Li, R. Long, Y. Ke, E. H. Sargent and Z. Ning, *Adv. Mater.*, 2019, **31**, 1903559.
13. Q. Cao, Y. Li, H. Zhang, J. Yang, J. Han, T. Xu, S. Wang, Z. Wang, B. Gao, J. Zhao, X. Li, X. Ma, S. M. Zakeeruddin, W. E. I. Sha, X. Li and M. Grätzel, *Sci. Adv.*, 2021, **7**, eabg0633.